Mechanical properties of aramid and UHMWPE thermoplastic composites: numerical and experimental trials

DOI: 10.35530/IT.075.05.202410

ALİ ARI
MEHMET KARAHAN
MUHAMMAD ALI NASİR

ABSTRACT – REZUMAT

Mechanical properties of aramid and UHMWPE thermoplastic composites: numerical and experimental trials

The out-of-plane behaviour of 8 different composites exposed to very high deformation rates and non-standard conditions was investigated in our previous studies. The mechanical properties of these composites have been evaluated through tests conducted at deformation rates comparable to those experienced during explosions. Based on the relevant test results, this study conducted a numerical analysis of 3 best-performing Aramid UD GS3000, Artec Aramid/Woven Aramid CT736, and H62 UD-UHMWPE-reinforced composites. In this regard, LS-DYNA's MAT54 model was compared with other failure mechanics-based models and preferred because it requires less experimental data and can simulate damage progression in dynamic failures. Since the samples used in the study were non-standard, quasi-static tensile and shear tests were performed based on the loads to which the composites would be exposed to create an accurate numerical analysis. Both tensile and shear strength values of the Artec Aramid/Woven Aramid CT736 composite are higher than those of the Aramid UD GS3000 and H62 UD-UHMWPE composites. When the numerical analysis results were compared with the tensile test data, compliance rates of 99.84% for Aramid UD GS3000 reinforced composite, 99.34% for Artec Aramid/Woven Aramid CT736 reinforced composite, and 96.42% for H62 UD-UHMWPE reinforced composite were determined. The analysis showed that the shear stress-strain curves provided 100% agreement at the maximum stress value.

Keywords: *numerical analysis, LS-DYNA, aramid, UHMWPE, quasi-static, shear test*

Proprietățile mecanice ale compozitelor termoplastice din fibre aramidice și UHMWPE: încercări numerice și experimentale

Comportamentul în afara planului a 8 compozite diferite expuse la rate foarte mari de deformare și la condiții non-standard a fost investigat în studiile noastre anterioare. Proprietățile mecanice ale acestor compozite au fost evaluate prin teste efectuate la rate de deformare comparabile cu cele experimentate în timpul exploziilor. Pe baza rezultatelor testelor relevante, acest studiu a efectuat o analiză numerică a 3 compozite armate cu cele mai ridicate performanțe, Aramid UD GS3000, Artec Aramid/Woven Aramid CT736 și H62 UD-UHMWPE. În acest sens, modelul MAT54 de la LS-DYNA a fost comparat cu alte modele bazate pe mecanica defecțiunilor și a fost preferat deoarece necesită mai puține date experimentale și poate simula progresia daunelor în defecțiuni dinamice. Deoarece eșantioanele utilizate în studiu au fost non-standard, au fost efectuate teste cvasi-statice de rezistenţă la tracțiune și la forfecare pe baza sarcinilor la care ar fi expuse compozitele, pentru a crea o analiză numerică precisă. Ambele valori ale rezistențelor la tracțiune și la forfecare ale compozitului Artec Aramid/Woven Aramid CT736 sunt mai mari decât cele ale compozitelor Aramid UD GS3000 și H62 UD-UHMWPE. Când rezultatele analizei numerice au fost comparate cu datele testului de rezistenţă la tracțiune, s-au determinat rate de conformitate de 99,84% pentru compozitul armat Aramid UD GS3000, 99,34% pentru compozitul armat Artec Aramid/Woven Aramid CT736 și 96,42% pentru compozitul armat H62 UD-UHM. Analiza a arătat că toate curbele de forfecare-deformare au atins rate de conformitate de 100% la valoarea maximă a tensiunii.

Cuvinte-cheie: *analiză numerică, LS-DYNA, aramidă, UHMWPE, cvasi-static, test de forfecare*

INTRODUCTION

Composite materials have been extensively employed as energy absorbers in various engineering domains, such as automotive and aerospace, owing to their exceptional ability to enhance the crashworthiness of structures and their lightweight properties [1]. Fibre-reinforced composites are the preferred choice compared to metallic absorbers because they possess greater stiffness, strength, and lower density. As a result, fibre-reinforced composite provides superior performance in terms of energy absorption per unit mass [2–4]. Furthermore, the brittle failure of composites involves various failure modes, including fibre failure, delamination, and matrix cracking. These failure modes significantly impact the overall performance of composites and provide challenges in the design and analysis of such systems [5]. As a result, there is a growing interest in analysing and evaluating the energy absorption

performances of composite using numerical simulations [6].

The intricate physical characteristics of failure modes displayed by laminated composite materials have posed a significant difficulty in numerically simulating these material systems beyond the elastic region. Crushing occurs when many failure modes, including matrix cracking, splitting, delamination, fibre tensile fracture, compressive kinking, frond production, bending, and friction, come together [7].

Given the current level of computer capacity, it is not feasible to encompass all of these failure modes inside a single analysis. Models utilizing lamina-level failure criteria have been employed, albeit with acknowledged constraints [8], to forecast the initiation of damage within laminate codes. After failure occurs, the process of failure propagation involves diminishing the material qualities through various degradation strategies [9]. To do dynamic impact analysis, such as crash analysis, it is essential to employ an explicit finite element code. This code solves the equations of motion numerically through direct integration using explicit methods, such as the central difference method [9]. LS-DYNA, ABAQUS Explicit, RADIOSS, and PAM-CRASH are commonly used software codes for conducting crash simulations [10]. Typically, these algorithms provide pre-existing material models for composites [11]. Each material model employs a distinct modelling approach, encompassing a failure criterion, degradation scheme, material properties, and frequently a collection of model-specific input parameters. These parameters are typically required for the computation but lack an immediate physical interpretation. Composites are represented as orthotropic linear elastic materials in the failure surface, which is determined by the chosen failure criterion in the model [9]. Outside of the failure surface, the suitable elastic characteristics experience degradation in accordance with degradation rules. The constitutive models can be categorized as either progressive failure models (PFM) or continuum damage mechanics models (CDM), depending on the specific degradation law employed. The LS-DYNA software package provides a range of material models for composite materials, including PFM (MAT22 and MAT54/55) and CDM (MAT58 and MAT162) [10]. In PFM, the failure criteria for laminated composites are often based on strength and employ a ply discount mechanism to reduce material characteristics. At the failure surface, the elastic characteristics of the ply in the material direction are reduced from their original undamaged state value of 1 to a wholly damaged state value of generally 0. The stress-strain curve of the material model does not necessitate the assignment of a specific unloading/softening curve. Once the strength of the ply is surpassed, the characteristics are instantaneously reduced to zero. The phenomenon known as progressive failure occurs when each layer of the laminate fails one by one, and once all layers have failed, the element is removed [12].

Extensive research has been conducted in the past twenty years on composites made from p-aramid and UHMWPE, as evidenced by numerous experimental investigations [13]. Models for the computational study of aramid-based woven and laminate structures have been devised and documented to assess the ballistic limit and layer-wise energy absorption [14]. A study by Hasanzadeh et al. [15] looked at numerical and experimental studies on ultra-high molecular weight polyethylene (UHMWPE) woven-based at 90 m/s projectile speed. The numerical results exhibited a high level of concurrence with the experimental findings. Liu et al. [16] created a computational model for body armour composed of UHMWPE fabric and soft materials and structures for absorbing energy. The numerical results exhibited a high degree of concordance with the experimental data. Scientists Haque et al. [17] used LS-DYNA to simulate the transverse impact on UHMWPE soft ballistic sublaminates. They used shell components and the MAT54 material model. The findings indicated that isotropic membranes exhibit a circular basal shape for the cone, while cross-ply laminates display a diamond shape. The validation process confirmed the accuracy of the finite element (FE) model by using both one-dimensional (UD) and two-dimensional (2D) theories to simulate transverse impact. Nilakantan and Nutt [18] investigated the impact of ply orientation and boundary conditions on the ballistic performance of p-aramid woven fabric. They employed a numerical model in LS-DYNA, which involved a rigid spherical projectile and varying numbers of woven fabric layers. Li et al. [19] created a FE model for combat helmets constructed from p-aramid woven fabric and phenolic resin. The model utilized orthotropic elasticity and a progressive damage model to accurately depict the minimized back-face signature. Wang et al. [20] conducted experiments and numerical simulations using LS-DYNA to study the effects of tensile and ballistic impacts on UHMWPE woven fabric. Their findings demonstrate a strong correlation between the experimental and numerical results. Obradovic et al. [21] investigated the impact of fibre-reinforced polymer composites' energy-absorbing structure employing MAT 54 and 55 in LS-Dyna simulations. Simulations of energy absorbers have demonstrated their ability to closely match experimental results, even when dealing with intricate geometries. Cherniaev et al. [22] tested how well three different material models – MAT 54, 58, and 262 – worked in LS-Dyna to model how composites collapse along their length. The study revealed that all the material models required significant calibration to reach a satisfactory agreement with the experimental findings. The models were calibrated using a trial-and-error methodology. Failure to calibrate the material properties resulted in substantial inaccuracies when predicting the behaviour of crushed composites.

In our previous studies, the energy absorption performances of various aramid and UHMWPE fabric-reinforced composites were examined with dynamic

pressure tests with the Split Hopkinson Pressure Bar (SHPB) method [23], Ballistic V50 [24] and various explosion tests [25–27]. In this study, 3 composites with the best performance according to the SPHB and Ballistic V50 test results will be selected, and numerical analysis of these composites will be carried out using the MAT54 model in LS-DYNA. In this process, quasi-static tensile and shear tests will be carried out to determine elastic-inelastic stress-strain behaviour and loss criteria to perform accurate numerical analyses of the composites. Finally, the numerical analysis results will be compared with experimental data.

MATERIALS AND METHODS

Materials

Four different fabrics (properties given in table 1) were used as reinforcement and nolax A21.2007 low-density polyethylene adhesive film (density 0.94 g/cm^3, melting temperature 80–90 °C and melt flow rate of 6–9 g/10 min) was used as the matrix system. The properties of fibres, which were used in the preparation of reinforcement structures, are given in table 2.

Composite manufacturing

The fabrics were cut to a size of 50 cm × 50 cm and composite laminates were prepared, with the same number of fabric layers and different panel thickness, different fabric layers and same panel thickness, different orientations of fabric layers and the same panel thickness and different number of fabric layers and different panel thickness, using the autoclave process. The temperature of the process was kept to 110°C and the pressure of the vacuum to 14.8 bar. Figure 1 shows the different stages of the manufacturing process. Table 3 gives detailed properties of the composites.

Fig. 1. Different stages of composite manufacturing process

Composite material models in LS-Dyna

Material properties like elastic modulus, shear modulus, and Poisson's ratio are needed for the input file. For failure analysis, strength properties such as

Table 1

PROPERTIES OF REINFORCEMENTS USED IN THE STUDY

Reinforcement type	Reinforcement code	Reinforcement producer	Weave type	Linear density of Warp/Fill yarns (Tex)		Warp/Fill (or 0°–90°) yarns		Yarn density (yarns/m)	Areal density (y/m^2)	Crimp Warp/Fill (%)	Reinforcement thickness (mm)
				Warp	Fill	Warp	Fill				
Aramid woven fabric- CT 736	R_1	Teijin	2×2 Basket weave	336/	336	Twaron 2000	Twaron 2000	127/127	410	0.8/0.8	0.6
Aramid woven fabric- Artec	R_2	Pro-System	1x1 Plain weave	58/	58	Artec	Artec	116/116	135	0.2/0.2	0.23
Aramid UD GS3000	R_4	FMS	UD	126	-	Kevlar 49/ Kevlar 49		-	510	Non-crimp	0.50
UHMWPE UD Dyneema H62	R_5	FMS	UD	176	-	Dyneema SK62		-	262	Non-crimp	0.25

Table 2

PARAMETERS OF THE ARAMID AND UHMWPE FIBERS USED IN THE STUDY

Parameters	Twaron 2000® (Aramid)	Kevlar 49® (Aramid)	Dyneema SK62® (UHMWPE)	Artec® Russian (Aramid)
Young modulus (GPa)	85	112	113	103
Strength (cN/Tex)	235	208	338	181
Ultimate elongation (%)	3.5	2.4	3.6	2.8
Density (g/cm^3)	1.44	1.44	0.97	1.44

Table 3

PROPERTIES OF THE COMPOSITE PLATES USED IN THIS STUDY

Sample code	Reinforcement type	Reinforcement layer number	Stacking direction	Resin	Plate thicknesses (mm)	Volume fraction (V_f)	Sample weight (g/m^2)
L1	R3	8	0°/90°	LDPE	3.9 ± 0.25	23.55	L1
L2	R1 + R2	12	0°/90°		4.1 ± 0.23	17.95	L2
L3	R4	12	0°/90°		3.8 ± 0.40	17.10	L3

longitudinal compressive strength, transverse compressive strength, longitudinal compressive strength, transverse tensile strength, and shear strength are needed. All the above-mentioned material models specifically deal with orthotropic materials. Every model has an option to determine the material axes, such as local and global orthotropic material axes. For a given geometry and load, the process of calculation is in three steps: (1) stress and strain distributions around the stress-concentrated areas are calculated; (2) failure (maximum) load is predicted; and (3) mode of failure is determined. The analysis consists of two major parts: stress analysis and failure analysis. The most often used material models are described with parametric studies to compare the differences.

Numerical analysis will be carried out with ANSYS LS-Dyna using the data obtained from the mechanical tests applied to the composites. There are many material models developed for composites in ANSYS LS-Dyna, and these models have different failure approaches, such as Chang and Chang [28], Hashin [29], and Tsai-Wu [30]. Considering the analysis method, element types, available test data, and comments in the literature, it has been seen that the most suitable material model for the purpose is *MAT_54_Enhanced_Composite_Damage. In this Mat_54, which has the Chang and Chang approach, damage can be modelled by decreasing the number of layers in multilayer elements and the corresponding decrease in elastic properties (Progressive Failure Model). The essential advantages of MAT_54 are its compatibility with the results obtained from experimental tests applied to composites and its usability in many different analyses.

Mechanical tests

Creating a material model is the most critical step in simulating an explosion accurately using finite element analysis. Material models are mathematical methods that developers base on the type of material and the loads it will be exposed to. These models include the elastic-inelastic stress-strain behaviour and loss criteria exhibited by the material under loading, and they are incorporated into the calculation when creating the element stiffness matrix.

Researchers obtain parameters for each material through experimental studies and include them in these models that encompass all material-related inputs. In numerical analyses where deformations are relatively low and commonly preferred materials are used academically or commercially, researchers can obtain material parameters from the literature. However, this study utilizes materials with very high deformation rates and non-standard materials. A meticulous experimental study can find the relevant parameters in this context. Before conducting numerical analysis and preparing material models, we subjected the composite layers, which are the last obstacle to transferring energy and force generated by the explosion to the human limb, to several mechanical tests.

Split Hopkinson pressure bar test

The out-of-plane behaviours of composites were examined in our study titled “Study of dynamic compressive behaviour of aramid and ultrahigh molecular weight polyethylene composites using Split Hopkinson Pressure Bar” [23], and the obtained data will be used in this study.

Tensile test

The in-plane mechanical behaviour of composite materials cannot be measured by the SHPB test. This is because, due to the low delamination resistance between layers, the planes show buckling behaviour as delamination rather than undergoing linear deformation under axial load. For this reason, in-plane SHPB test results performed for trial purposes showed very low strength, and it was understood that it could not be used when creating the material model.

The in-plane tensile behaviour of the composite layers was ensured by conventional composite tensile testing by ASTM D3039 standards. The tests were carried out under quasi-static conditions using an extensometer at room temperature (figure 2), and in-plane stress-strain graphs of the composites were created with the results. Tensile test samples were prepared by cutting in the 0° direction.

Shear test

Since the elastic material behaviour of composites is modelled using the orthotropic approach, it is necessary to know the independent shear moduli (G) in three directions. Composite layers will be modelled with two-dimensional shell elements in the finite element model. Therefore, finding the in-plane shear modulus (G_{12}) will be sufficient. Shear tests of the 3 materials determined by the SHPB test and samples prepared by ASTM D7078 standards (figure 3) were carried out (figure 4). The test utilizes a special

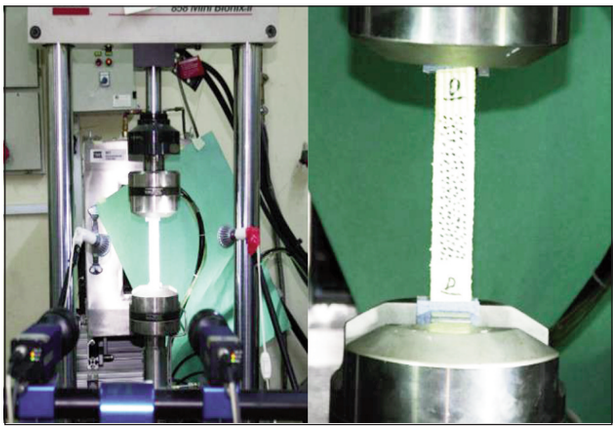

Fig. 2. Quasi-static test setups, tensile testing by using a clip-on biaxial extensometer (MTS Bionix II Axial test system)

fixing device to expose the samples, cut with a water jet, to pure shear according to the ASTM D7078 standard, resulting in the measurement of shear stress-shear strain.

MAT_54 enhanced composite damage model

MAT_54 is a model developed for multilayer UD and woven materials with orthotropic behaviour. In this model, which can work with Shell and Tshell (thick shell) elements in ANSYS LS-Dyna, elastic behaviours in fibre (1) and lateral (2) directions, two different elastic coefficients (E_{11}, E_{22}), planar Poisson ratio (ν_{12}) and the shear modulus in three directions (G_{12}, G_{23}, G_{31}) (equation 1–3).

$$\varepsilon_{11} = \frac{1}{E_{11}}(\sigma_{11} - \nu_{12}\varepsilon_{22}) \quad (1)$$

$$\varepsilon_{22} = \frac{1}{E_{22}}(\sigma_{22} - \nu_{21}\varepsilon_{11}) \quad (2)$$

$$2\varepsilon_{12} = \frac{1}{G_{12}}\tau_{12} + \alpha\tau_{12}^{3} \quad (3)$$

Out-of-plane elastic behaviour in multi- and thin-layered structures is unimportant and can be ignored because loading in this direction results in bending instead of axial deformation. For this reason, models developed for this type of material, such as MAT_54, do not include out-of-plane elastic parameters and are assumed to be rigid in the thickness direction. Thanks to this assumption, the number of 9 independent parameters in the orthotropic approach was reduced to 6 by removing the parameters E_{33}, ν_{23}

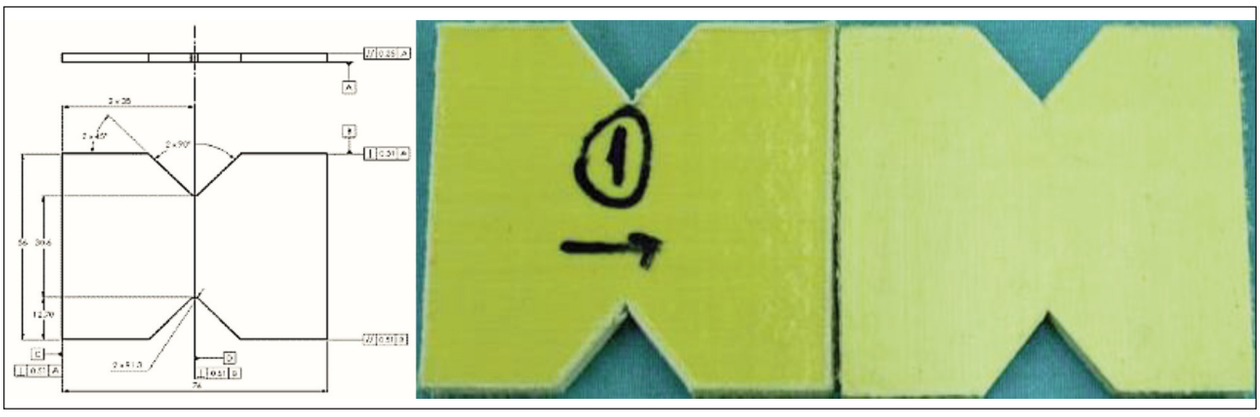

Fig. 3. Schematic representation of the sample shape specified in ASTM D7078 and an example of a composite sample prepared in accordance with this standard

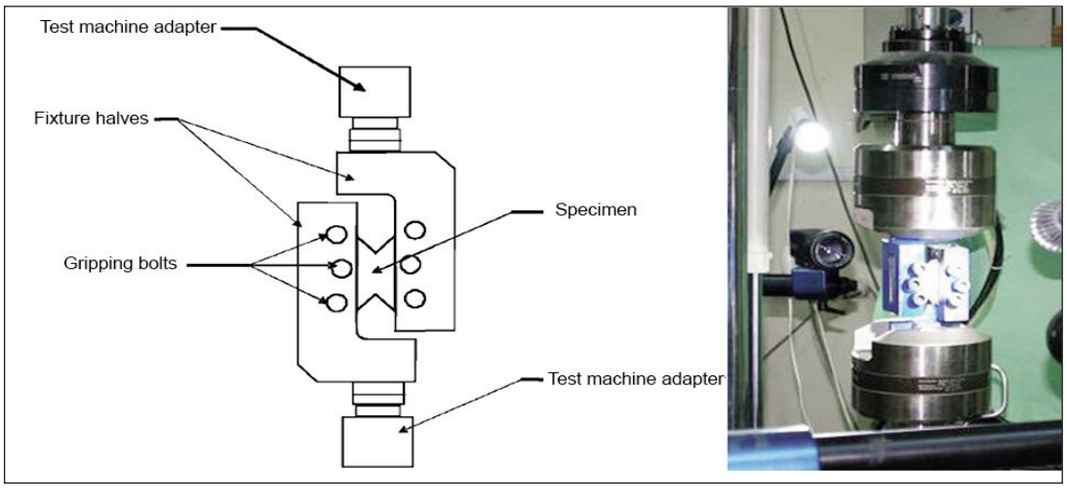

Fig. 4. Polymer-based shear test schematic and apparatus in accordance with ASTM D7078 standard

and ν_{31}. This has eliminated the need for out-of-plane mechanics, which makes it very difficult to prepare samples and obtain high-accuracy results. Although MAT_54 requires elastic shear modulus in three directions, it does not calculate the out-of-plane shear modulus (G_{23}, G_{31}) separately and assumes it to be equal to the in-plane shear modulus (G_{12}) [7, 31–33]. The planar shear strain (ε_{12}) calculation uses the nonlinear α parameter to adapt to the nonlinear shear stress-shear strain curve.

The point distinguishing the MAT_54 model from other composite material models is the modelling phase of damage and fracture behaviour. In the damage criterion developed by Chang and Chang, each layer is subjected to fracture independently of the others, and with this fracture, weakening occurs. Beyond the elastic region, MAT_54 uses the Chang-Chang [28] failure criterion to determine individual ply failure, as given by equations 4–7. In the following equations, e_f, e_c, e_m and ed are called history variables, and they are failure flags that represent (respectively) tension and compression for the fibre direction and tension and compression for the matrix direction. Failure: It is achieved by defining the critical stress separately for compression (XC) and tension (XT) in the fibre direction and for compression (YC) and tension (XT) in the lateral direction. Additionally, users can input the critical shear stress (SC).

The tensile fracture in the fibre direction is given in equation 4.

$$e_t^2 = \left(\frac{\sigma_{11}}{X_T}\right)^2 + \beta\left(\frac{\sigma_{12}}{S_c}\right)^2 - 1 \begin{cases} < 0, & \text{elastic} \\ \geq 0, & \text{failed} \end{cases} \quad (4)$$

When the failure occurs, E_{11}, E_{22}, G_{12}, and ν_{12} become equal to 0. The coefficient β is the parameter that adjusts the effect of plane shear stress on the failure in the fibre direction. While $\beta = 1$ is the Hashin failed criterion, $\beta = 0$ is the ideal maximum fibre stress criterion. The selected value depends on the test results.

The compressive failure in the fibre direction is given in equation 5:

$$e_c^2 = \left(\frac{\sigma_{11}}{X_c}\right)^2 - 1 \begin{cases} < 0, & \text{elastic} \\ \geq 0, & \text{failed} \end{cases} \quad (5)$$

Upon failure: $E_{11} = \nu_{12} = \nu_{21} = 0$.

Tensile failure in the matrix (lateral) direction is given in equation 6:

$$e_m^2 = \left(\frac{\sigma_{22}}{Y_T}\right)^2 + \beta\left(\frac{\sigma_{12}}{S_c}\right)^2 - 1 \begin{cases} < 0, & \text{elastic} \\ \geq 0, & \text{failed} \end{cases} \quad (6)$$

Upon failure: $E_{11} = G_{12} = \nu_{12} = 0Y_c$

The failure under lateral compressive load is given in equation 7:

$$e_d^2 = \left(\frac{\sigma_{22}}{2S_c}\right)^2 + \left[\left(\frac{Y_c}{2S_c}\right)^2 - 1\right]\frac{\sigma_{22}}{Y_c} + \left(\frac{\sigma_{12}}{S_c}\right)^2 - 1 \begin{cases} < 0, & \text{elastic} \\ \geq 0 & \text{failed} \end{cases} \quad (7)$$

Upon failure: $E_{22} = \nu_{21} = \nu_{12} = 0 = G_{12} = 0$.

All specified elastic properties are set to zero when one of the above conditions is exceeded in a ply within the element. If any of these criteria are met, the program calculates the stresses in the next time step using new coefficients and adds them to the current stress record, along with the reset elastic coefficients. The stresses are not eliminated by failure; instead, the increasing stress is limited in the face of increasing load. Furthermore, if a failure happens in the relatively weaker matrix (lateral) direction, it is also possible to model the weakening in the fibre direction. The FBRT parameter provides this attenuation with a value between 0 and 1, and equations 8 and 9 determine the tensile strength (XT) and/or compressive strength (XC) in the fibre direction.

$$XT = XT * FBRT \quad (8)$$

$$XC = XC * FBRT \quad (9)$$

As mentioned before, when the current stress criteria in the model are met, the reset elastic coefficients are valid for that time step, and the stresses are not reset. In MAT_54, complete zeroing of stresses is achieved by strain criteria, and these criteria are entered separately for tension (DFAILT) and compression (DFAILC) in the fibre direction, compression (DFAILM) in the matrix (lateral) direction, and planar shear (DFAILS). When any of these criteria are met, all stresses in the layer drop to 0 (figure 5). Additionally, critical equivalent strain (EFS) can be defined independently of direction, and if the strain in any direction exceeds this value, the stresses become 0. Once the stresses in all element layers reach zero, the element is permanently deleted.

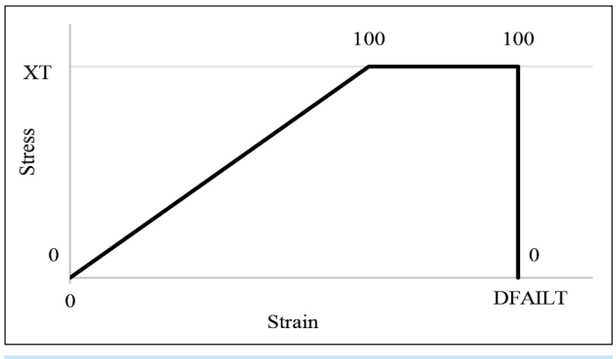

Fig. 5. MAT_54 fibre direction stress-strain curve form

Determination of material parameters

Planar tensile and shear tests determined the plane's elastic parameters and failure criteria. It is important to note that mechanical tests are independent of fibre or lateral direction. It is important to note that mechanical tests are independent of fibre or lateral direction. This is because all composites' layer orientations are [0°/90°]; thus, they show the same mechanical behaviour in the 11 and 22 directions. Each layer's fibre direction was placed at a 90° angle to the one above and below it and subjected to mechanical testing. Putting the fibre direction in each

layer at a right angle to the layers above and below it and testing it mechanically made sure that the damage criteria and elastic coefficients that were put in when the material model was made stayed the same.

RESULTS AND DISCUSSION

According to the results of our previous studies, the SHPB test was applied to 8 different composite samples [23]. As a result of comparing these 8 different materials, 3 samples were selected. Due to variations in their elastic properties and shape-changing speeds, not all composites could be tested at the same reference deformation rates. The reason for this is that even though they are tested with the same gas pressure, the elastic properties of the materials are not the same, and they change shape at different speeds. This caused the comparison to be made at low, medium, and high deformation rates rather than at a single reference deformation rate. As a result of the data obtained from the previous study [23], Woven Aramid CT-736/Bi-axial Aramid, Woven Aramid CT736, H5T UD-UHMWPE, and UD-Aramid/H62 UD-UHMWPE-reinforced composites were eliminated due to their low energy absorption at moderate deformation rates. UD-Aramid/UD-UHMWPE-reinforced composite was excluded from the scope because it is hybrid and showed low toughness compared to H62 UD-UHMWPE-reinforced composite in quasi-static tests. When Stabond UD-Aramid and GS3000 UD-Aramid were compared at low deformation rates, it was seen that they gave similar results, and the results of V50 tests were used [34]. As a result of the V50 tests, the GS300 UD-Aramid-reinforced composite was significantly more successful, and the Stabond UD-Aramid-reinforced composite was eliminated.

After the elimination, 3 composite materials remained used in numerical analyses and explosion tests. These materials, GS300 UD-Aramid (L1), H62 UD-UHMWPE (L3), and Artec Aramid/Woven Aramid CT736 (L2), showed high strength in all tests. Consequently, the study [35] utilized these three materials in various combinations for the numerical explosion analysis and ongoing tests. The stress-strain graphs at different deformation rates, which were obtained using SHPB test results [23] and which will be used as references in the numerical analysis of these composite materials, are given in figure 7, respectively. The parameters and approaches obtained from these graphs will be discussed in detail.

Tensile test

The SHPB test cannot measure the in-plane mechanical behaviour of composite materials. This is because, due to the low delamination resistance between layers, the planes show buckling behaviour as delamination rather than undergoing linear deformation under axial load. As a result, the in-plane SHPB test results demonstrated insufficient strength, rendering them unsuitable for incorporation into the material model.

When the stress-strain graphs for the plane of the 3 materials selected for the continuation of the study are examined (figure 7), it is seen that L2 has a tensile strength value that is 2.2 times higher than L1 and 1.5 times higher than L3.

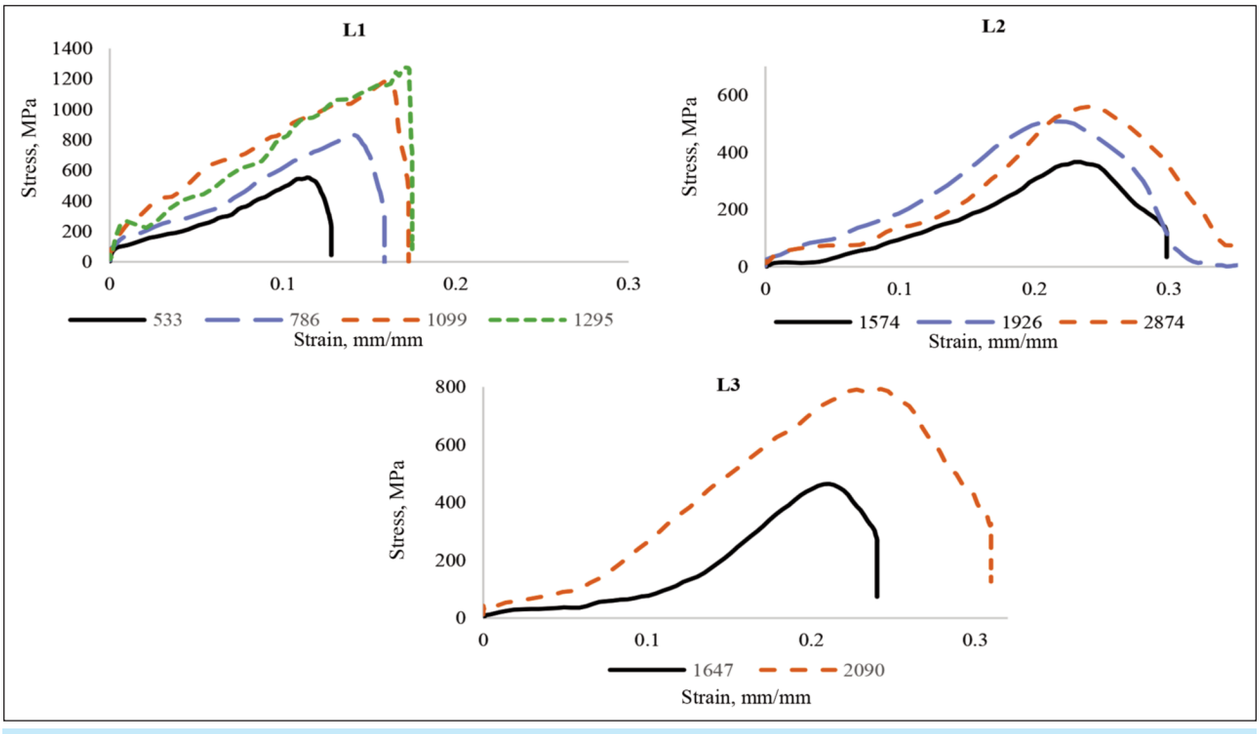

Fig. 6. Out-of-plane stress-strain at different deformation rates (1/s) of Aramid UD GS3000 [0°/90°], Artec Aramid/Woven Aramid CT736 [0°/90°], and H62 UD-UHMWPE [0°/90°] composites curves

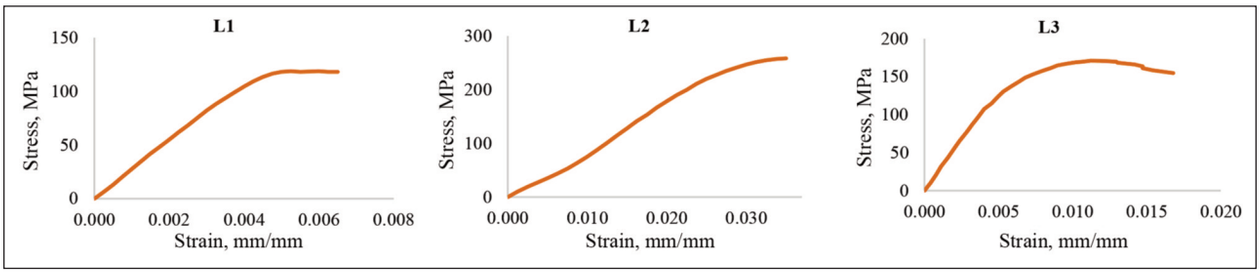

Fig. 7. Planar stress-strain curves obtained by tensile testing of Aramid UD GS3000 [0°/90°], Artec Aramid/Woven Aramid CT736 [0°/90°], and H62 UD-UHMWPE [0°/90°] composites

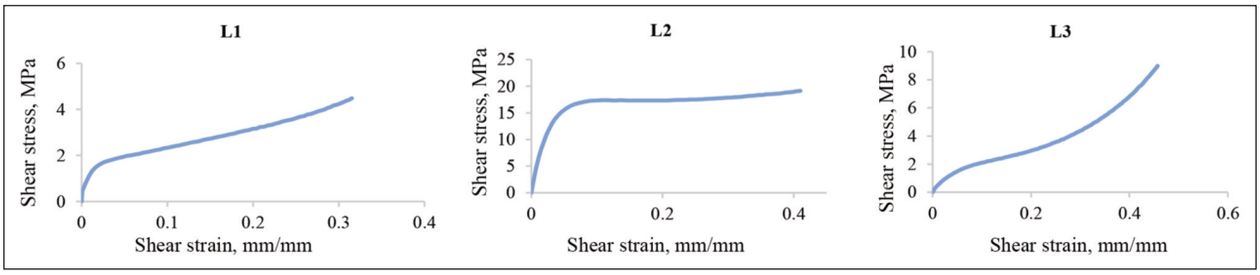

Fig. 8. Plane shear stress-shear strain curves of Aramid UD GS3000 [0°/90°], Artec Aramid/Woven Aramid CT736 [0°/90°], and H62 UD-UHMWPE [0°/90°] composites

Shear test

When the shear stress-shear strain graphs obtained as a result of the shear tests, Figure 8, are examined, it is seen that L2 has a shear strength value that is 4.3 times higher than L1 and 2.2 times higher than L3.

Description of the baseline MAT54 model

The MAT_54 model parameters obtained from the test results of three composite materials are shown in table 4. No values are defined for the parameters not included in table 6, and the default values are accepted as correct.

In the numerical analysis of the current study, the composites were modelled using multiple shell pieces on top of each other instead of a single shell piece, and the contacts mentioned were defined between each shell piece and the ones above and below it. The failure parameters of the contacts were determined as the stress in the normal direction (option=4, NFLS), and the maximum stress values obtained in the SHPB test were used as the value.

Table 4

MAT_54 MODEL PARAMETERS OF THE MATERIALS TO BE USED IN THE ANALYSIS					
	LS-Dyna Variables	**Parameters**	**Stabond UD-Aramid**	**Artec Aramid / Aramid CT736**	**H62 UD-UHMWPE**
Elastic behaviour	EA (E_{11}) (MPa)	Young's modulus fibre directions	25106.4	8125	27500
	EB (E_{22}) (MPa)	Young's modulus lateral directions	25106.4	8125	27500
	PRAB (ν_{12})	Poisson ratio	0.148	0.864	0.006
	GAB (G_{12}) (MPa)	Shear modulus (in-plane)	300	1000	45
	GCA (G_{31}) (MPa)	Shear modulus (out-of-plane)	300	1000	45
	GBC (G_{23}) (MPa)	Shear modulus (out-of-plane)	300	1000	45
	ALPH (α)	Shear stress non-linear term	$3.3 \cdot 10^{-3}$	$5.5 \cdot 10^{-5}$	$3.6 \cdot 10^{-4}$
Failure parameters	XT (MPa)	Longitudinal tensile strength	118	260	165
	YT (MPa)	Transverse tensile strength	118	260	165
	SC (MPa)	Shear strength	8.99	19.13	4.49
	EFS (mm/mm)	Effective failure strain	0.47	0.41	0.32
	BETA (β)	Weighing factor for the shear term in tensile fibre mode	0.5	0.5	0.5
	DFAILT (mm/mm)	Max strain for fibre tension	0.0065	0.035	0.017
	DFAILM (mm/mm)	Max strain for matrix straining in tension and compression	0.0065	0.035	0.017
	DFAILS (mm/mm)	Max shear strain	0.47	0.41	0.32

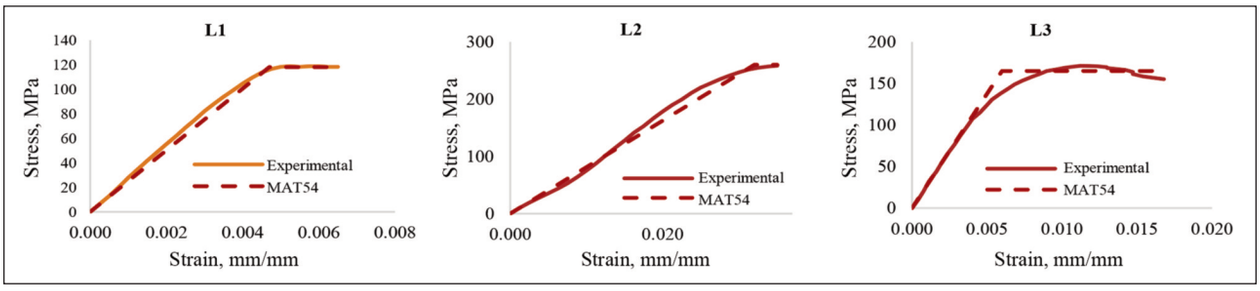

Fig. 9. Ideal bilinear curves generated on tensile test data for material model MAT_54 of Aramid UD GS3000 [0°/90°], Artec Aramid/Woven Aramid CT736 [0°/90°], and H62 UD-UHMWPE [0°/90°]

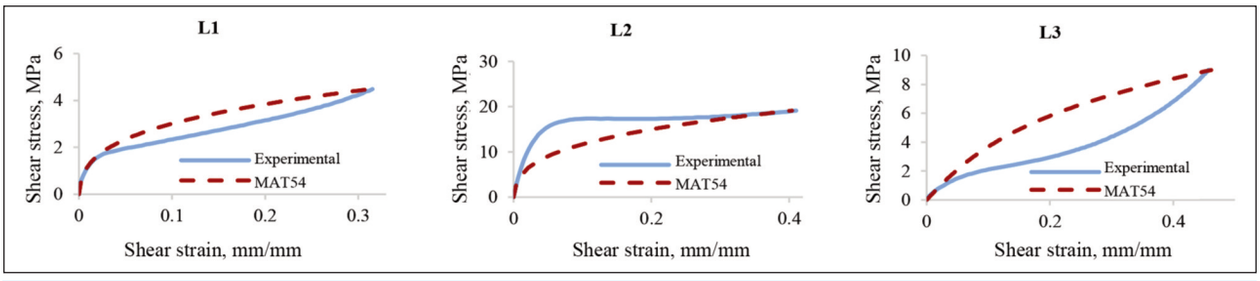

Fig. 10. Idealized shear stress-shear strain curves for MAT_54, Aramid UD GS3000 [0°/90°], Artec Aramid/Woven Aramid CT736 [0°/90°], and H62 UD-UHMWPE [0°/90°]

While elastic coefficients and failure parameters were determined, ideal bilinear curves were created based on the tensile test results (figure 9). The slope of the first part of these curves, representing the elastic region, is determined as the elastic modulus (E_{11} and E_{22}). The stress value at which the curve becomes horizontal is the failure stress (XT and YT), while the strain value at which the curve becomes zero is the failure strain (DFAILT and DFAILM). Considering the geometric deformation of the composite under explosion, the damage criteria in the compression direction were unnecessary and set to 0. To prevent possible element distortion or stability problems arising from this assumption, we entered the same value as DFAILS in the EFS parameter.

When figure 9 and table 5 are examined, it is seen that the experimental and numerical analysis results of the L1, L2, and L3 samples are in reasonable agreement with the maximum stress value.

Shear modulus (G12), α parameter (ALPHA), and shear strength (SC) values were determined based on the shear stress-shear strain results of the materials. Equation 10 polynomial was drawn on the result curves, and the A and B coefficients that best fit the curve were determined (figure 10).

$$\gamma = A\tau + B\tau^3 \quad (10)$$

The shear modulus (G12) was entered as the value obtained for A, and the α parameter (ALPHA) was entered as the value obtained for B.

The stress levels in the numerical analysis of the L1, L2, and L3 samples in figure 10 did not match the experimental data at first, but as they got closer to the maximum stress (table 6), they became more in line with the experimental data.

Out-of-plane mechanical behaviour

As mentioned, the MAT_54 model does not contain elastic parameters or failure criteria for out-of-plane elastic behaviour. Although out-of-plane axial elastic deformation is not essential, delamination may occur due to high-speed loading in this direction. Defining breakable contacts between elements, regardless of the material model, achieves modelling of this damage. The literature frequently uses this approach [33], which utilizes the specially developed *Contact_Automatic_One_Way_Surface_To_Surface_Tie_Break

Table 5

COMPARISON OF LS-DYNA PREDICTIONS TO TEST FOR ULTIMATE FAILURE STRESS			
Samples	**Experimental ultimate failure stress (MPa)**	**Numerical ultimate failure stress (MPa)**	**Percent difference (%)**
L1	118.186	118	0.16
L2	258.290	260	–0.66
L3	171.120	165	3.58

Table 6

COMPARISON OF LS-DYNA PREDICTIONS TO TEST FOR ULTIMATE FAILURE SHEAR STRESS			
Samples	**Experimental ultimate shear stress (MPa)**	**Numerical ultimate shear stress (MPa)**	**Percent difference (%)**
L1	4.48	4.48	0.00
L2	19.13	19.13	0.00
L3	8.9	8.9	0.00

contact in ANSYS LS-Dyna. Since these contacts do not meet the failure parameters, they transfer the axial and shear loads in tension and compression to the other part. When the failure parameters are met, separation between the parts is allowed, and force transfer in the sliding direction occurs only through shear. These criteria can be force, tension, or energy loss.

CONCLUSIONS

The most crucial stage in successfully simulating an explosion using finite element analysis is developing a material model. In this context, the Split Hopkinson Pressure Bar test performed in previous studies determined the out-of-plane behaviour of composites. Based on this data, numerical analysis of GS3000 UD-Aramid, H62 UD-UHMWPE, and Artec Aramid/Woven Aramid CT736 reinforced composites, which have the highest energy absorption performance, was performed with LS-DYNA MAT54. In-plane elastic parameters and failure criteria were determined by tensile and shear tests.

According to the tensile test, the Artec Aramid/Woven Aramid CT736 reinforced composite exhibited the best performance, showing a tensile strength value that was 2.2 times higher than the Aramid UD GS3000 reinforced composite and 1.5 times higher than the H62 UD-UHMWPE reinforced composite.

According to the shear test, the Artec Aramid/Woven Aramid CT736 reinforced composite exhibited the best performance, showing a shear strength value that was 4.3 times higher than the Aramid UD GS3000 reinforced composite and 2.2 times higher than the H62 UD-UHMWPE reinforced composite.

The debonding contact algorithm between adjacent layers and the MAT54 composite material model used for each shell layer showed high performance in the numerical analysis of composite laminates in LS-Dyna. When the analysis results were compared with the stress-strain curves obtained from the tensile test data, it was observed that the Aramid UD GS3000 reinforced composite had a compliance rate of 99.84%, the Artec Aramid/Woven Aramid CT736 reinforced composite had a compliance rate of 99.34%, and the H62 UD-UHMWPE reinforced composite had a compliance rate of 96.42%. However, initially, there was a mismatch in the shear stress-strain curves, but then 100% agreement was achieved at the maximum stress value. The comparison shows high accuracy in the analysis despite the phenomenon's complexity.

REFERENCES

[1] Baroutaji, A., Sajjia, M., Olabi, A.G., *On the Crashworthiness Performance of Thin-Walled Energy Absorbers: Recent Advances and Future Developments*, In: Thin-Walled Struct., 2017, 118, 137–163, https://doi.org/10.1016/J.TWS.2017.05.018

[2] Zhang, Z., Sun, W., Zhao, Y., Hou, S., *Crashworthiness of Different Composite Tubes by Experiments and Simulations*, In: Compos. Part B Eng., 2018, 143, 86–95, https://doi.org/10.1016/J.COMPOSITESB.2018.01.021

[3] Karahan, M., Yildirim, K., *Low Velocity Impact Behaviour of Aramid and UHMWPE Composites*, In: Fibres Text. East. Eur., 2015, 23, 97–105, https://doi.org/10.5604/12303666.1152522

[4] Hazra, K., Harper, J.F., *Damage Tolerance Behaviour of Carbon Fibre Multi-Axial Warp Knit Fabric Composites*, In: Int. J. Veh. Struct. Syst., 2011, 3, 192–202, https://doi.org/10.4273/ijvss.3.3.07

[5] Kumar, Y., Rezasefat, M., Hogan, J.D., *Axial Crushing of Circular Thin-Walled Specimens Made of CFRP Using Progressive Failure Model (MAT54) in LS-Dyna*, In: Mater. Today Proc., 2023, https://doi.org/10.1016/ j.matpr.2023.01.354

[6] Zhao, X., Zhu, G., Zhou, C., Yu, Q., *Crashworthiness Analysis and Design of Composite Tapered Tubes under Multiple Load Cases*, In: Compos. Struct., 2019, 222, 110920, https://doi.org/10.1016/J.COMPSTRUCT. 2019.110920

[7] Feraboli, P., Wade, B., Deleo, F., Rassaian, M., Higgins, M., Byar, A., *LS-DYNA MAT54 Modeling of the Axial Crushing of a Composite Tape Sinusoidal Specimen*, In: Compos. Part A Appl. Sci. Manuf., 2011, 42, 1809–1825, https://doi.org/0.1016/j.compositesa.2011.08.004

[8] Hinton, M.J., Kaddour, A.S., Soden, P.D., *A Comparison of the Predictive Capabilities of Current Failure Theories for Composite Laminates, Judged against Experimental Evidence*, In: Compos. Sci. Technol., 2002, 62, 1725–1797, https://doi.org/10.1016/S0266-3538(02)00125-2

[9] Xiao, X., *Modeling Energy Absorption with a Damage Mechanics Based Composite Material Model*, In: Journal of Composite Materials, 2009, 43, 427–444, http://dx.doi.org/10.1177/0021998308097686

[10] Rahman, S.A., Ashraf, M., Subhani, M., Reiner, J., *Comparison of Continuum Damage Models for Nonlinear Finite Element Analysis of Timber under Tension in Parallel and Perpendicular to Grain Directions*, In: Eur. J. Wood Wood Prod., 2022, 80, 771–790, https://doi.org/10.1007/s00107-022-01820-8

[11] Ozturk, U.E., Anlas, G., *Finite Element Analysis of Expanded Polystyrene Foam under Multiple Compressive Loading and Unloading*, In: Mater. Des., 2011, 32, 773–780, https://doi.org/10.1016/j.matdes.2010.07.025

[12] Zhang, Y., Zhou, Y., Lu, Z., *Evaluation of Failure Criteria for Composite Plate under High-Velocity Impact*, In: J. Mech. Sci. Technol., 2022, 36, 3291–3300, https://doi.org/10.1007/s12206-022-0609-5

[13] Ari, A., Karahan, M., Kopar, M., Ahrari, M., *The Effect of Manufacturing Parameters on Various Composite Plates under Ballistic Impact*, In: Polym. Polym. Compos., 2022, 30, 1–15, https://doi.org/10.1177/09673911221144874

[14] Zhou, Y., Li, H., Zhang, Z., Li, G., Xiong, Z., Wang, M., *Ballistic Response of Stitched Woven Fabrics with Superior Energy Absorption Capacity: Experimental and Numerical Investigation*, In: Compos. Struct., 2021, 261, 113328, https://doi.org/10.1016/J.COMPSTRUCT.2020.113328

[15] Hasanzadeh, M., Mottaghitalab, V., Rezaei, M., Babaei, H., *Numerical and Experimental Investigations into the Response of STF-Treated Fabric Composites Undergoing Ballistic Impact*, In: Thin-Walled Struct., 2017, 119, 700–706, https://doi.org/10.1016/J.TWS.2017.07.020
[16] Liu, X., Li, M., Li, X., Deng, X., Zhang, X., Yan, Y., Liu, Y., Chen, X., *Ballistic Performance of UHMWPE Fabrics/EAMS Hybrid Panel*, In: J. Mater. Sci., 2018, 53, 7357–7371, https://doi.org/10.1007/S10853-018-2055-4/FIGURES/13
[17] Haque, B.Z.G., Ali, M.A., Gillespie, J.W., *Modeling Transverse Impact on UHMWPE Soft Ballistic Sub-Laminate*, In: J. Thermoplast. Compos. Mater., 2017, 30, 1441–1483
[18] Nilkantan, G., Nutt, S., *Effects of Ply Orientation and Material on the Ballistic Impact Behavior of Multilayer Plain-Weave Aramid Fabric Targets*, In: Def. Technol., 2018, 14, 165–178, https://doi.org/10.1016/J.DT.2018.01.002
[19] Li, Y.Q., Li, X.G., Gao, X.L., *Modeling of Advanced Combat Helmet under Ballistic Impact*, In: J. Appl. Mech. Trans. ASME, 2015, 82, https://doi.org/10.1115/1.4031095/474229
[20] Wang, H., Weerasinghe, D., Mohotti, D., Hazell, P.J., Shim, V.P.W., Shankar, K., Morozov, E.V., *On the Impact Response of UHMWPE Woven Fabrics: Experiments and Simulations,* In: Int. J. Mech. Sci., 2021, 204, 106574, https://doi.org/10.1016/J.IJMECSCI.2021.106574
[21] Obradovic, J., Boria, S., Belingardi, G., *Lightweight Design and Crash Analysis of Composite Frontal Impact Energy Absorbing Structures*, In: Compos. Struct., 2012, 94, 423–430, https://doi.org/10.1016/J.COMPSTRUCT.2011.08.005
[22] Cherniaev, A., Butcher, C., Montesano, J., *Predicting the Axial Crush Response of CFRP Tubes Using Three Damage-Based Constitutive Models*, In: Thin-Walled Struct., 2018, 129, 349–364, https://doi.org/10.1016/J.TWS.2018.05.003
[23] Shaker, K., Jabbar, A., Karahan, M., Karahan, N., Nawab, Y., *Study of Dynamic Compressive Behaviour of Aramid and Ultrahigh Molecular Weight Polyethylene Composites Using Split Hopkinson Pressure Bar*, In: J. Compos. Mater., 2017, 51, 81–94, https://doi.org/10.1177/0021998316635241
[24] Karahan, M., Jabbar, A., Karahan, N., *Ballistic Impact Behavior of the Aramid and Ultra-High Molecular Weight Polyethylene Composites*, In: J. Reinf. Plast. Compos., 2014, 34, 37–48, https://doi.org/10.1177/0731684414562223
[25] Karahan, M., Karahan, N., *Development of an Innovative Sandwich Composites for the Protection of Lower Limbs against Landmine Explosions*, In: J. Reinf. Plast. Compos., 2016, 35, 1776–1791, https://doi.org/10.1177/0731684416668261
[26] Karahan, M., Karahan, E.A., *Development of an Innovative Sandwich Composite Material for Protection of Lower Limb against Landmine Explosion: Mechanical Leg Test Results*, In: Text. Res. J., 2016, 87, 15–30, https://doi.org/10.1177/0040517515624880
[27] Kamberoğlu, M., Karahan, M., Alpdoğan, C., Karahan, N., *Evaluation of Foot Protection Effectiveness against AP Mine Blasts: Effect of Deflector Geometry*, In: J. Test. Eval., 2017, 45, 356–368, https://doi.org/10.1520/JTE20150171
[28] Chang, F.K., Chang, K.Y., *Post-Failure Analysis of Bolted Composite Joints in Tension or Shear-Out Mode Failure*, In: Journal of Composite Materials, 1987, 21, 809–833, https://doi.org/10.1177/002199838702100903
[29] Hashin, Z., *Failure Criteria for Unidirectional Fiber Composites*, In: J. Appl. Mech., 1980, 47, 329–334, https://doi.org/10.1115/1.3153664
[30] Tsai, S.W., Afb, W.-P., Wu, E.M., Louis, S., *A General Theory of Strength for Anisotropic Materials*, In: Journal of Composite Materials, 1971, 5, 58–80, https://doi.org/10.1177/002199837100500106
[31] Krishnamoorthy, S., *Prediction of Structural Response of Frp Composites for Conceptual Design of Vehicles Under Impact Loading*, Ls-Dyna®, 2011, 96
[32] Wade, B., Feraboli, P., Osborne, M., *Simulating Laminated Composites Using LS-DYNA Material Model MAT54 Part I : [0] and [90] Ply Single-Element Investigation*, In: FAA Jt. Adv. Mater. Struct. Cent. Excell. Tech. Rev. Meet., 2012, 33
[33] Heimbs, S., Heller, S., Middendorf, P., *Simulation of Low Velocity Impact on Composite Plates with Compressive Preload*, In: LS-DYNA Anwenderforum, 2008, 11–24
[34] Karahan, M., Jabbar, A., Karahan, N., *Ballistic Impact Behavior of the Aramid and Ultra-High Molecular Weight Polyethylene Composites*, In: J. Reinf. Plast. Compos., 2015, 34, 37–48, https://doi.org/10.1177/ 0731684414562223
[35] Karahan, M., Karahan, E.A., *Development of an Innovative Sandwich Composite Material for Protection of Lower Limb against Landmine Explosion: Mechanical Leg Test Results*, In: Text. Res. J., 2017, 87, 15–30, https://doi.org/10.1177/0040517515624880

Authors:

ALİ ARI[1], MEHMET KARAHAN[2,3], MUHAMMAD ALİ NASİR[4]

[1]Department of Weapon Industry Technician, Vocational School of Higher Education, Ostim Technical University, 06374, Ankara, Türkiye

[2]Vocational School of Technical Sciences, Bursa Uludag University, 16059, Bursa, Türkiye
e-mail: mkarahan@uludag.edu.tr

[3]Butekom Inc., Demirtas Dumlupinar OSB District, 2nd Cigdem Street No:1/4, 16245, Osmangazi, Bursa, Türkiye

[4]University of Engineering and Technology, Department of Mechanical Engineering, Taxila, Pakistan

Corresponding author:

ALİ ARI
e-mail: ali.ari@ostimteknik.edu.tr